



This is a repository copy of *Techno-economic evaluation of post-combustion carbon capture based on chemical absorption for the thermal cracking furnace in ethylene manufacturing*.

White Rose Research Online URL for this paper:

<https://eprints.whiterose.ac.uk/197560/>

Version: Accepted Version

Article:

Hu, G., Li, X., Liu, X. et al. (7 more authors) (2023) Techno-economic evaluation of post-combustion carbon capture based on chemical absorption for the thermal cracking furnace in ethylene manufacturing. *Fuel*, 331 (Part 2). 125604. ISSN 0016-2361

<https://doi.org/10.1016/j.fuel.2022.125604>

Article available under the terms of the CC-BY-NC-ND licence (<https://creativecommons.org/licenses/by-nc-nd/4.0/>).

Reuse

This article is distributed under the terms of the Creative Commons Attribution-NonCommercial-NoDerivs (CC BY-NC-ND) licence. This licence only allows you to download this work and share it with others as long as you credit the authors, but you can't change the article in any way or use it commercially. More information and the full terms of the licence here: <https://creativecommons.org/licenses/>

Takedown

If you consider content in White Rose Research Online to be in breach of UK law, please notify us by emailing eprints@whiterose.ac.uk including the URL of the record and the reason for the withdrawal request.



eprints@whiterose.ac.uk
<https://eprints.whiterose.ac.uk/>

1 Techno-economic evaluation of post-combustion carbon capture based on chemical
2 absorption for the thermal cracking furnace in ethylene manufacturing
3

4 Guihua Hu^a, Xiaoxu Li^a, Xiaoyan Liu^a, Jun Hu^b, Olajide Otitoju^c, Meihong Wang^{a,c*}, Wenli Du^{a*},
5 Zhencheng Ye^a, Jian Long^a, Feng Qian^a

6 ^a Key Laboratory of Smart Manufacturing in Energy Chemical Process, Ministry of Education, School of
7 Information Science and Engineering, East China University of Science and Technology, Shanghai 200237, China

8 ^b School of Chemistry and Molecular Engineering, East China University of Science and Technology, Shanghai
9 200237, China

10 ^c Department of Chemical and Biological Engineering, The University of Sheffield, Sheffield S1 3JD, United
11 Kingdom

12 *Corresponding author Email addresses: meihong.wang@sheffield.ac.uk
13

14 **Abstract:**

15 As the core equipment of ethylene production plant, thermal cracking furnace generates a large amount of CO₂
16 emissions. To reduce the CO₂ emissions, post-combustion carbon capture based on monoethanolamine (MEA)
17 solvent is used to capture CO₂ from the thermal cracking furnace. The computational fluid dynamics (CFD)
18 method was used to simulate the operation of a 60kt/a thermal cracking furnace to obtain the flow rate and
19 composition of the flue gas. A carbon capture plant model was carried out using Aspen Plus[®] and validated using
20 the Technology Centre Mongstad (TCM) pilot plant data. Scale-up of the capture plant model was carried out to
21 match the flue gas flow rate of the thermal cracking furnace. Two integration cases of the carbon capture plant and

22 the industrial thermal cracking unit were carried out. The results show that the excess heat of the gasoline
23 fractionator can be used to provide heat for the carbon capture plant without affecting ethylene production. The
24 economic evaluation was conducted based on the two case studies. Results show that the cost of CO₂ capture can
25 be reduced from \$80.03/tonne without heat integration to \$70.41/tonne with heat integration of gasoline
26 fractionators with carbon capture plant. When considering the impact of carbon credits on capture costs, the cost
27 will be further reduced to \$50.41/tonne.

28 **Keywords:** Thermal cracking furnace; solvent-based post-combustion carbon capture; computational fluid dynamics; heat integration;
29 economic evaluation

30

31 **1. Introduction**

32 1.1. Background

33 Due to the development of world industry, greenhouse gas emissions have been on the increase. CO₂ is the main
34 greenhouse gas. In 2019, CO₂ emissions from fossil fuel burning reached 88.6% of the total greenhouse gas
35 emissions [1]. Due to this, CO₂ emissions have attracted widespread attention. As the largest carbon emitter
36 worldwide, China accounts for 28.8% of the world's total energy carbon emissions [2]. Therefore, it is urgent for
37 China to reduce CO₂ emissions if it is to meet its target of achieving carbon neutrality by 2060.

38 Ethylene is one of the most extensively used chemical products in the world. In 2020, the worldwide ethylene
39 production capacity reached 197 million tonnes/year [3]. China is the second-largest producer of ethylene in the
40 world [4]. During the cracking of naphtha to ethylene, 1.73 tonnes of CO₂ is emitted for each tonne of ethylene
41 produced [5]. The industrial thermal cracking furnace is the core equipment of the ethylene industry. It generates

42

Nomenclature		\vec{r}	position vector
a^l	total interfacial area for mass transfer, m^2	R	universal gas constant
a_p	special area of the packing, m^2/m^3	R_i	net rate of production of species i by chemical reaction, $kgmol/m^3/s$
a_v	total area of packing per unit volume, m^2/m^3	\vec{s}	direction vector
a_w	surface area of wetted packing per unit volume of packing, m^2/m^3	\vec{s}'	scattering direction vector
A	empirical constants, 4.0	S	slant height of a corrugation, m
A_t	cross-sectional area of the column, m^2	T	temperature, °C
B	empirical constants, 0.5	U_i, U_j, U_l	velocity component in the i th, j th or l th direction, m/s
C_l	a dimensionless constant which depends on the packing size	V_{CC}	value of carbon credit, \$/tonne
$C_{1\varepsilon}$	standard k - ε model constant, 1.44	$V_{G,fl}$	flooding velocity, m/s
$C_{2\varepsilon}$	standard k - ε model constant, 1.92	V_G	superficial gas velocity, m/s
C_c	CO ₂ capture cost, \$/tonne	x_i, x_j, x_l	coordinate direction in the i th, j th or l th direction, m
C_{cc}	CO ₂ capture cost with carbon credit, \$/tonne	Y_P	mass fraction of any product species, P
C_{cm}	mass flow of the captured CO ₂ , kg/s	Y_R	mass fraction of a particular reactant, R
$C_{j,r}$	molar concentration of species j in reaction r , $kgmol/m^3$	Greek letters	
d_p	effective diameter of packing, m	α	absorption coefficient, 1/m
D	diameter, m	α_{Rich}	rich loading, mol CO ₂ /mol MEA
D_{Ag}	gas phase diffusivity of CO ₂	α_{Lean}	lean loading, mol CO ₂ /mol MEA
D_{Al}	liquid phase diffusivity of CO ₂	ε	Ddissipation rate of turbulent kinetic energy, m^2/s^3
E_a	average annual capital cost, \$	θ	angel with horizontal of falling film or corrugation channel
F_p	packing factor, m^{-1}	μ	viscosity of gas molecules, kg/m s
F_t	correction factor for total holdup due to effective wetted area	μ_g	gas dynamic viscosity (Pa s)
g_{eff}	effective gravity, m/s^2	μ_l	Liquid dynamic viscosity (Pa s)
G	gas mass flow rate, kg/s	μ_s^l	superficial velocity for the liquid, m/s
G_k	generation of turbulent kinetic energy, $J/m^3/s$	ρ	gas density, kg/m^3
h_L	volumetric liquid holdup, m^3	ρ_G	gas density, kg/m^3
h_p	height of the packed section, m	ρ_L, ρ_l^l	liquid density, kg/m^3
h_i	fractional holdup	Γ	net effect of third bodies on the reaction rate
I	radiation intensity, $J/m^2/s$	ν	kinematic viscosity, m^2/s
k	turbulent kinetic energy, m^2/s^2	$\nu'_{i,r}$	stoichiometric coefficient for reactant i in reaction r
$k_{f,r}$	forward rate constant for reaction r	$\nu''_{i,r}$	stoichiometric coefficient for product i in reaction r
k_g	gas film mass transfer coefficient, m/s	$\eta'_{j,r}$	rate exponent for reactant species j in reaction r
k_l	liquid film mass transfer coefficient, m/s	$\eta''_{j,r}$	rate exponent for product species j in reaction r

K_{eq}	equilibrium constant, -	σ	Stefan-Boltzmann constant, $5.672 \times 10^{-8} \text{W/m}^2\text{K}^4$
L	solvent mass flow rate, kg/s	σ_S	scattering coefficient, 1/m
M_{MEA}	molar mass of MEA, kg/kmol	σ_k	standard k - ϵ model constant, 1.0
M_{wi}	molecular weight of species i , kg/kgmol	σ_ϵ	standard k - ϵ model constant, 1.3
n	refractive index	φ_{CO_2}	percentage of CO_2 captured
N	number of chemical special in the system	Φ	phase function
OM_a	average annual operating cost, \$	ω_{MEA}	MEA concentration, wt%
ΔP_f	flooding pressure drop, in H_2O /ft	Ω'	solid angle

43

44 large amounts of CO_2 with concentrations of 7-10 mol% in the flue gas. Therefore, a significant measure to reduce
 45 CO_2 emissions from the ethylene plants is to capture the CO_2 produced by the thermal cracking furnace.

46 Several approaches such as oxy-fuel combustion, pre-combustion, and post-combustion can be used for CO_2
 47 capture[6]. Post-combustion capture technology can be used to capture CO_2 from the flue gas released from large
 48 stationary sources such as ethylene or power plants without making radical changes to existing plants. The
 49 difficulties accompanying its implementation are lower compared to the other capture approaches. Although CO_2
 50 separation technologies such as adsorption, membrane and cryogenic separation are used for post-combustion
 51 capture, The liquid absorption-based CO_2 capture is the most matured technology and the most widely used in
 52 commercial applications. The MEA based post-combustion CO_2 capture also has high CO_2 capture efficiency
 53 (>90%) and CO_2 high purity (>99%) [7]. The adsorption method has low energy consumption and high reliability,
 54 however, the adsorption capacity and selectivity of the adsorbent are low[8], particularly at low adsorption
 55 pressures. The working environment of the membrane separation method is relatively strict, and it lacks stability
 56 in a complex environment. Further to this, it is still in the research and development stage. Because MEA has high
 57 absorption and separation characteristics for CO_2 , it is suitable for treating flue gas with low CO_2 partial pressure[9].
 58 Therefore, the post-combustion carbon capture (PCC) process with MEA solvent is adopted in this research.

59 1.2. Previous research

60 There are many studies on the simulation of the thermal cracking furnace. Zhou and Yang [10] established and
61 optimized a convection section calculation model of the ethylene cracking furnace, which can calculate the
62 temperature and heat duty of the convection section tube row. For the fire side, Hottel and Sarofim [11] presented
63 the zone method initially applied to simulate the radiative heat transfer process [12, 13]. In the past few decades,
64 because of the development of computational fluid dynamics (CFD) and the sharp rise in computing power, CFD
65 has become a favorite tool to simulate the thermal cracking furnace. Many CFD simulation studies have
66 investigated the flow, combustion, radiative heat transfer processes, and the NO_x and CO emissions of the furnaces
67 [14-18]. For the process gas side, during the last decades, the research on the modeling of cracking reactions has
68 developed from molecular reaction models [19, 20] to free radical reaction models [21-24], which has made
69 tremendous progress. Findings from these studies, showed that CFD can simulate and correctly predict the detailed
70 concentration of each component of the flue gas from the furnace, including the concentration of CO produced by
71 partial incomplete combustion. This makes the concentration of the components obtained by CFD calculation to
72 be more accurate compared to other simulation tools such as Aspen Plus® which only considers rapid reaction and
73 is unable to simulate partial incomplete reaction. In this paper, the cracking furnace is simulated using the CFD
74 method.

75 Over the past few decades, many researchers have investigated solvent-based PCC technology. Zhang et al. [25]
76 developed a rigorous carbon capture plant model and validated the model using pilot plant data from the University
77 of Texas at Austin. Their results indicated that the high heat duty of the reboiler in the stripper could hinder the
78 widespread large-scale implementation of the liquid absorbent-based PCC process. To reduce the reboiler duty,
79 Freguia and Rochelle [26] conducted sensitivity analyses of the process variables in the CO₂ capture process to
80 analyze the impact of operating conditions on the steam requirement. Wang et al. [6] pointed out that proper process

81 integration could reduce the energy consumption of the PCC process. Tatarczuk et al. [27] used an inter-heated
82 stripper to modify the process of split flow. The pilot trials showed that while the CO₂ capture efficiency was
83 increased by 8-12%, the regeneration duty was reduced by 8-11%.

84 The integration of PCC with coal-fired power plants (CFPP) has been widely studied [28-31]. Liu et al. [32]
85 developed steady-state models for MEA-based PCC process and supercritical CFPP and set up different integration
86 cases to study the performance of thermal integration. Wei et al. [33] developed an integrated model of an industrial
87 fluid catalytic cracking unit and a PCC plant with MEA solvent. They investigated the effect of different heat
88 integration cases on energy consumption. Wu et al. [34] presented a coordinated control strategy for integrating
89 the combined-cycle gas turbine power plant with solvent-based PCC process and considered the influence of
90 disturbances. Chen et al. [35] accomplished an economic optimization for CFPP integrated with PCC process. The
91 overall plant revenue increased using the proposed scheduling. Xi et al. [36] presented a parametric optimization
92 in terms of absorber/stripper size and operating conditions for solvent-based PCC process, where flexible operation
93 of the CFPP was considered.

94 For CO₂ capture from the ethylene industry, Weikl and Schmidt [37] presented a techno-economic study of CO₂
95 capture from the ethylene production plant. They compared the CO₂ capture performance between the oxyfuel-
96 combustion and post-combustion process in the cracking furnace. Zhao et al.[38] selected ethylene as the research
97 object to study the low-carbon roadmap of chemical production. The emission reduction potential of different
98 ethylene production routes was compared. So far, no study has put forward a detailed integration model of a carbon
99 capture plant with an ethylene production plant.

100 1.3. Motivation and novelty

101 Previous researches have focused on integrating solvent-based PCC plants with refineries and power plants to

102 reduce CO₂ emissions. However, considering the importance of ethylene manufacturing in the global economy
103 and the accompanying huge carbon emissions, it is imperative to intensify efforts at cutting down CO₂ emissions
104 from this process by integrating it with solvent-based PCC plant. As with the integration of solvent-based PCC
105 plant with power plants and refineries, the energy consumption and the cost of the solvent-based PCC plant
106 integrated with ethylene plant needs to be quantified. In addition to this, various integration schemes that could
107 lead to a reduction in the energy consumption and cost of the process needs to be explored.

108 To this end, this study evaluates the energy consumption and costs of the solvent-based PCC plant integrated
109 with an ethylene plant based on two integration methods namely No Heat Integration and Heat Integration of
110 Gasoline Fractionators in thermal cracking. The no heat integration method involves the use of purchased low-
111 pressure steam for solvent regeneration when the ethylene plant is integrated with the PCC plant. The heat
112 integration of gasoline fractionator on the other hand involves the use of hot oil to generate the saturated steam
113 that is used for solvent regeneration.

114 Additionally, economic evaluation of the two proposed integration methods is conducted to evaluate their
115 capacity and cost to reduce CO₂ emissions.

116 The specific novelties of this work can be summarized as follow:

117 (1) Detailed scale-up of the solvent-based PCC plant based on a flue gas from a commercial thermal cracking
118 furnace is carried out for the first time.

119 (2) Assessments of the energy consumption of the solvent-based PCC plant integrated with an ethylene plant
120 based on the no heat integration strategy and a novel heat integration of the gasoline fractionators in thermal
121 cracking.

122 (3) A detailed economic assessment of the solvent-based PCC plant based on the two integration strategies is

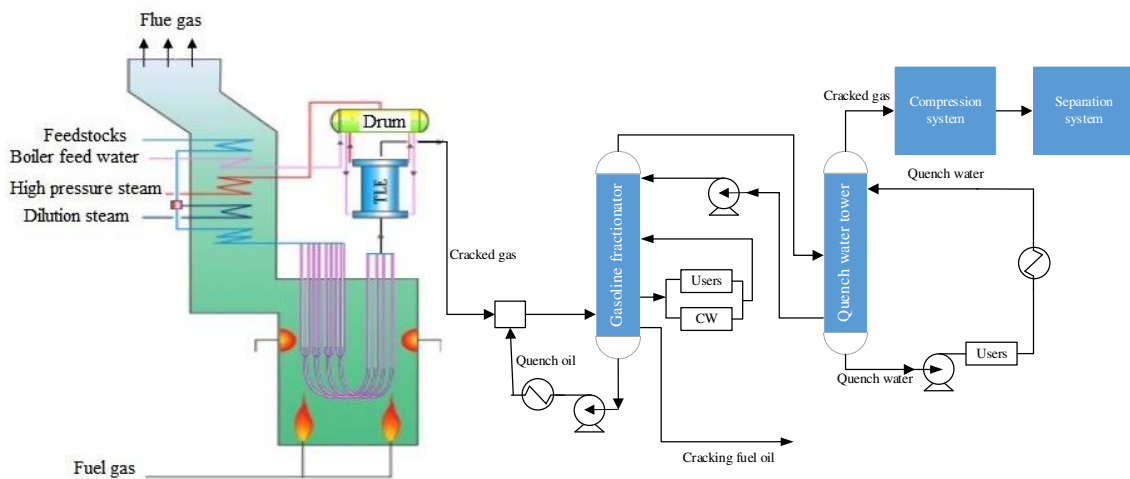
123 performed using the equipment costs, operating costs, and carbon credits as performance indicators.

124 2. Process description and model development for the thermal cracking unit

125 2.1. Description of the thermal cracking unit

126 The thermal cracking unit processes various petroleum hydrocarbon feedstocks such as naphtha and propane
127 into ethylene and propylene under high-temperature conditions. The thermal cracking furnace is the core of a
128 thermal cracking unit. Fig.1 shows a typical industrial thermal cracking unit.

129 In a thermal cracking furnace, the convection section serves to recover the heat of flue gas, preheat, and vaporize
130 the hydrocarbon feedstock. The hydrocarbon feedstock and dilution steam are heated in the tubes of the convection
131 section. When the temperature reaches the incipient cracking temperature, they enter the reactor tubes in the middle



132
133 **Fig. 1. Typical arrangement of an industrial thermal cracking unit.**

134 of the radiation section, where the cracking reactions occur. Fuel gas combustion in the radiation section outside
135 the reactor tubes provides the heat required for the cracking reactions. The burners are arranged at the bottom of
136 the firebox and/or on both sides of the side walls. Fuel gas and air enter the firebox through the burners. The
137 released heat is mainly transferred to the medium in the reactor coils by radiation and convection [16]. The quench
138 system includes steam drum and transfer line heat exchanger (TLE). After cracking quickly, the process gas leaves

139 the reactor coils to TLE and is rapidly cooled by heat exchange with the saturated water from the steam drum. The
140 cracking gas from TLE flows into the main pipe and is sent to the gasoline fractionator after oil quenching. In the
141 gasoline fractionator, quench oil is used to cool the cracking gas further and recover the heat of the cracking gas.
142 The heat of the pan oil in the middle of the gasoline fractionator is recovered by low-grade heat users and the
143 circulating water (CW). The users include heat exchangers and materials that need to be heated. After oil washing,
144 the cracked gas enters the quench water tower for further cooling. The quench water after heat exchange with the
145 cracked gas is used to provide heat to the low-level heat users. The cooled cracked gas enters the compression
146 system and separation system for further processing.

147 2.2. Model development for the thermal cracking unit

148 As described above, the thermal cracking unit consists mainly of the radiation and convection sections.
149 Therefore, to develop an accurate model of the thermal cracking unit, detailed and complete models of the radiation
150 section and the convection section are required. In the current work, the convection section and radiation section
151 of a 60kt/a industrial thermal cracking furnace are simulated using the CFD method. More detailed and elaborate
152 descriptions of the models and governing equations used for the convection section have been presented in Hu et
153 al. [39] and those used for the radiation section are available in Hu et al. [16]. For the sake of brevity and clarity,
154 they are briefly described in the following subsections.

155 2.2.1. Radiation section

156 A coupled simulation of the radiation section of the thermal cracking unit was carried out using the models for
157 the turbulence flow, combustion, radiative heat transfer and thermal cracking reaction processes. The turbulence
158 flow model is based on the standard k- ϵ two equations presented in Eq. (1) and Eq. (2) [16].

$$159 \quad k - \text{equation:} \quad \frac{\partial}{\partial x_i} (\rho k U_i) = \frac{\partial}{\partial x_j} \left[\left(\mu + \frac{\mu_t}{\sigma_k} \right) \frac{\partial k}{\partial x_j} \right] + G_k - \rho \epsilon \quad (1)$$

$$\varepsilon - \text{equation: } \frac{\partial}{\partial x_i} (\rho k \varepsilon U_i) = \frac{\partial}{\partial x_j} \left[\left(\mu + \frac{\mu_t}{\sigma_\varepsilon} \right) \frac{\partial \varepsilon}{\partial x_j} \right] + \frac{\varepsilon}{k} (C_{1\varepsilon} G_k - C_{2\varepsilon} \rho \varepsilon) \quad (2)$$

The fuel gas combustion is described using the finite-rate/eddy-dissipation model [16]. This model computes the chemical source terms using the Arrhenius expressions. In other words, the net production of chemical species i due to reaction can be expressed as the sum of the Arrhenius reaction sources over the reactions N_R as follows:

$$R_i = M_{w,i} \sum_{r=1}^{N_R} \hat{R}_{i,r} \quad (3)$$

$\hat{R}_{i,r}$ is the Arrhenius molar rate of creation/destruction of species i in reaction r . It is calculated using Eq. (4).

$$\hat{R}_{i,r} = \Gamma(v_{i,r}'' - v_{i,r}') \left(k_{f,r} \prod_{j=1}^N [C_{j,r}]^{(\eta_{j,r} + \eta_{j,r}'')} \right) \quad (4)$$

The net rate of specie i production due to reaction r ($R_{i,r}$) is given by the limiting value of the two expressions in Eq. (5) and Eq. (6).

$$R_{i,r} = v_{i,r}' M_{w,i} A \rho \frac{\varepsilon}{k} \min \left(\frac{Y_R}{v_{i,r}' M_{w,i}} \right) \quad (5)$$

$$R_{i,r} = v_{i,r}' M_{w,i} A B \rho \frac{\varepsilon}{k} \frac{\sum p Y_p}{\sum_j v_{j,r}'' M_{w,j}} \quad (6)$$

The Discrete Ordinates (DO) model presented in Eq.(7) is used to calculate radiative heat transfer of the furnace [16].

$$\nabla \cdot (I(\vec{r}, \vec{s}) \vec{s}) + (\alpha + \sigma_s) I(\vec{r}, \vec{s}) = \alpha n^2 \frac{\sigma T^4}{\pi} + \frac{\sigma_s}{4\pi} \int_0^{4\pi} I(\vec{r}, \vec{s}') \Phi(\vec{s}, \vec{s}') d\Omega' \quad (7)$$

The cracking process in the reactor coils of the radiation section is simulated using the one-dimensional reactor model COILSIM1D [39, 40].

2.2.2. Convection section

The model of the convection section consists of the models of the convection chamber and the tubes. The turbulence flow in the convection chamber is modeled using the k - ε models described in Eq. (1) and Eq. (2). Likewise, the radiative heat transfer is modeled with the DO model described in Eq. (7). In the tubes of convection

180 section, the renormalization group (RNG) k- ϵ model and the volume of fluid (VOF) model [39] are used to simulate
 181 the turbulence flow, and the liquid-vapor two phases flow, respectively. A summary of the geometry and operating
 182 conditions of the thermal cracking unit is shown in Table 1, and a comparison between simulation results and
 183 industrial data is shown in Table 2.

184 **Table 1 Summary of the thermal cracking geometry and operating conditions**

Radiation section specifications			
Length (x direction) (m)	10.368	Length (y direction) (m)	3.55
Length (z direction) (m)	14.27		
Number of bottom burners	24	Number of side burners	64
Convection chamber specifications			
Length (x direction) (m)	10.368	Length (y direction) (m)	2.26
Length (z direction) (m)	13.385		
Number of tube sections	8	Number of total tubes	432
Firing condition			
Fuel gas flow rate in bottom (kg/h)	2682	Fuel gas flow rate in side (kg/h)	1788
Excess air (V%)	1.1		
Fuel composition (mol%)			
CH ₄	93.55	H ₂	6.08
C ₂ H ₄	0.14	C ₂ H ₆	0.083
C ₃ H ₈	0.062	C ₄ H ₁₀	0.065
C ₅	0.020		
Material properties			
Emissivity of the furnace wall	0.75	Emissivity of tube skin	0.85

Feedstock composition (wt%)			
n-Paraffins	30.16	i-Paraffins	41.56
Olefins	1.37	Naphthenes	16.13
Aromatics	10.78		

185 According to the relative error percentage between the simulation results and the industrial data, it can be seen
186 that the model accurately simulates the operation of the industrial ethylene cracking furnace. The simulated results
187 of the outlet temperature and flue gas compositions from the thermal cracking unit are reported in Table 3.

188 **Table 2 Comparison between simulation results and industrial data**

Items	Simulation results	Industry data	Relative error %
Flue gas outlet temperature of radiation section (°C)	1179	1191	1.01
Propene-to-ethene ratio (wt%/wt%)	0.50	0.50	0
Combustion heat load (MW)	62.56	62.70	0.22
Radiation efficiency (%)	41.02	40.14	2.19
Convection heat load (MW)	32.19	33.86	4.93

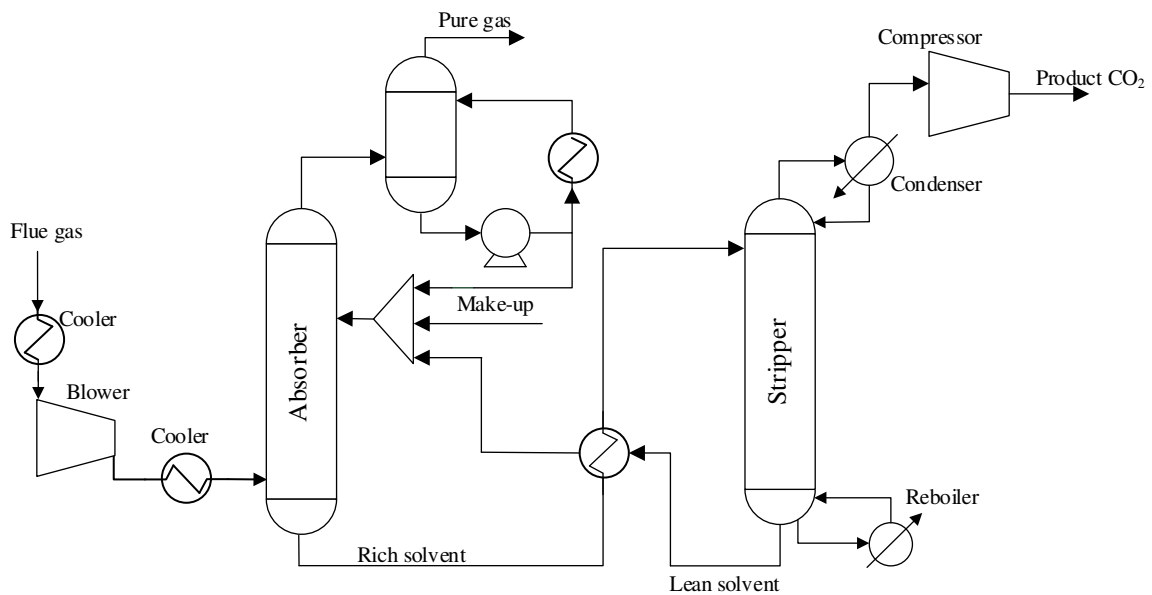
189 **Table 3 Simulated flue gas components and temperature**

Variable	Value
Outlet temperature (°C)	115.50
Outlet pressure (kPa)	101.3026
Flow rate (kg/s)	24.72
Mole composition	
O ₂ (mol%)	3.87
H ₂ O (mol%)	15.60
CO ₂ (mol%)	7.69
N ₂ (mol%)	72.84

190 **3. Process description and model development and model validation of the CO₂**
191 **capture plant**

192 3.1. CO₂ capture plant description

193 The reference capture process used is the standard process shown in Fig.2 [26]. The flue gas entering the
194 absorber from the cracking furnace contains components such as Oxygen, water, carbon dioxide and nitrogen (as
195 shown in Table 3). It is assumed that particulates, NO_x and SO_x have been removed from the flue gas prior to
196 entering the absorber. The temperature of the flue gas is cooled with heat exchanger before and after being
197 pressurized in the blower to aid the absorption process . The flue gas is cooled to between 30-40 °C before entering
198 the absorber. . The flue gas enters the bottom of the absorber while the lean solvent enters the absorber from the
199 top. In the countercurrent process, the CO₂ is absorbed, and the treated flue gas is discharged from the top of the
200 absorber. The treated flue gas contains an amount of water and MEA. After recovering the water and MEA from
201 the washing column, the pure gas is discharged into air. The rich solvent leaves the absorber from the bottom and
202 is pumped into the stripper for regeneration after being heated by a cross-heat exchanger. After regeneration, the
203 solvent is returned to the absorber from the bottom of the stripper. The high-purity CO₂ released from the top of
204 the stripper is compressed and stored.

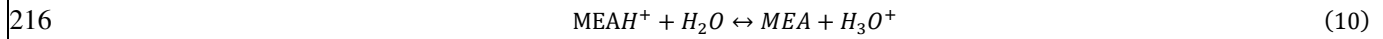
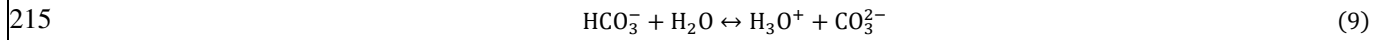
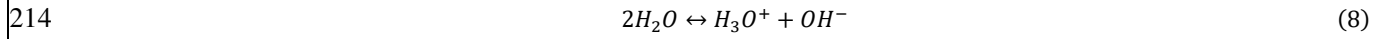


205
206 **Fig. 2. Schematic diagram of carbon capture process based on MEA solution**

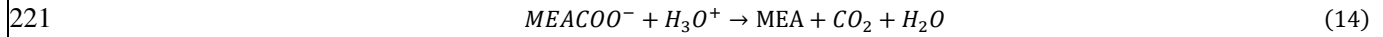
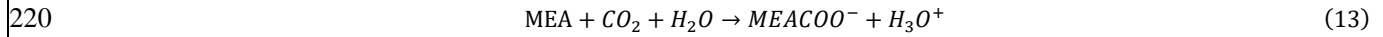
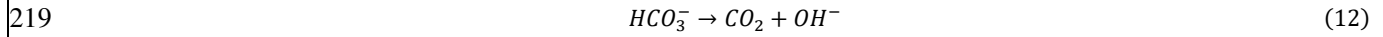
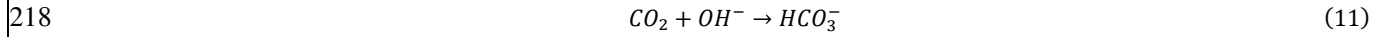
207 3.2. Model development of CO₂ capture plant

208 The CO₂ capture model was developed using Aspen plus V11[®]. The RadFrac block was used to model the
209 absorber and stripper. The liquid phase properties are calculated by the Electrolyte Non-Random-Two-Liquid
210 (ELECNRTL) model and the gas phase properties are calculated with the Redlich-Kwong (RK) equation of state
211 [41]. In this paper, the kinetic model proposed by Aboudehir et al. [42] and AspenTech [43] were used. The
212 equilibrium and rate-controlled reactions describing the absorption of CO₂ by MEA are as follows:

213 The equilibrium reactions:



217 The rate-controlled reactions:



222 The equilibrium constant K_{eq} of reactions (8)-(10) was determined based on molar concentration using the
223 expression in Eq. (15):

$$224 \quad \ln(K_{eq}) = A + \frac{B}{T} + C \cdot \ln(T) + D \cdot T \quad (15)$$

225 The kinetic expression of reactions (11)-(14) is:

$$226 \quad r = kT^n \exp\left(-\frac{E}{RT}\right) \prod_{i=1}^N C_i^{a_i} \quad (16)$$

227 The values of the parameters for the equilibrium reactions and rate-controlled reactions are shown in Table 4.

228 For the absorber and stripper in the CO₂ capture model, the same packing type and size as the pilot plant are used.

229 The parameters of the pilot plant will be described in section 3.3.

230 The gas-film and liquid-film mass transfer coefficients are obtained from the widely used correlations provided

231 by Onda et al.[44]:

$$232 \quad \frac{k_g RT}{a_v D_{Ag}} = C_1 \left(\frac{G}{a_v \mu_g} \right)^{0.7} \left(\frac{\mu_g}{\rho_g D_{Ag}} \right)^{1/3} (a_v d_p)^{-2.0} \quad (17)$$

233

$$234 \quad k_l \left(\frac{\rho_l}{\mu_l g} \right)^{1/3} = 0.0051 \left(\frac{L}{a_\omega \mu_l} \right)^{2/3} \left(\frac{\mu_l}{\rho_l D_{Al}} \right)^{-0.5} (a_v d_p)^{0.4} \quad (18)$$

235 The interfacial area for mass transfer is provided by the study of Bravo et al.[45]:

$$236 \quad a^I = a_p A_t h_p \quad (19)$$

237 The liquid holdup in structured packing is provided by Bravo et al.[46]:

$$238 \quad h_L = h_t h_p A_t \quad (20)$$

$$239 \quad h_t = \left(4 \frac{F_t}{S} \right)^{2/3} \left(\frac{3 \mu^L u_s^L}{\rho_t^L g_{eff} \varepsilon \sin \theta} \right)^{1/3} \quad (21)$$

240 **Table 4 Coefficients of equilibrium constants and kinetic parameters [41]**

	A	B	C	D
Eq.(8)	132.889	-13455.9	-22.477	0
Eq.(9)	216.049	-12431.7	-35.482	0
Eq.(10)	-3.038	-7008.36	0	-0.00313
	K		E (cal/mol)	
Eq.(11)	4.32e+13		13,249	
Eq.(12)	2.38e+17		29,451	
Eq.(13)	9.77e+10		9855.8	

Eq.(14)

2.18e+18

14138.4

241 3.3. Model validation of the CO₂ capture plant

242 The CO₂ Technology Centre Mongstad (TCM) located in Bergen is the largest test facility for CO₂ capture
243 technology globally. The TCM pilot plant is designed to be flexible and can test different configurations. The
244 capture plant can treat flue gas from residual fluid catalytic crackers with a CO₂ content of approximately 13-14
245 vol%. It can also treat flue gas with 3.5vol% CO₂ from the combined heat and power (CHP) plant. When processing
246 the flue gas from the CHP plant, the primary equipment data of the TCM carbon capture plant is listed in Table 5.
247 The CHP plant has a flue gas flow rate of 60000 Sm³/h and can capture 80 tonnes of CO₂ per day[47]. There is an
248 absorption column equivalent to a diameter of 3 m for the CO₂ absorption into MEA solvent, and the packing
249 height is up to 24 m. The performance of the carbon capture plant was tested in 2014 and 2015 with 30wt% MEA
250 as solvent [48, 49]. Table 6 provides the main process information of the CO₂ capture plant during the averaged
251 base-case test period. The detailed gas composition data is from Øi and Fagerheim[50].

252 **Table 5 Column specifications of the absorber and stripper in the TCM carbon capture pilot plant**

	Absorber	Stripper
Geometry	Rectangular	Cylindrical
Cross-sectional area (m ²)	7.1	1.33
Packing type	Koch Glitsch Flexipac 2X	Koch Glitsch Flexipac 2X
Packing height (m)	24	8

253 The model is validated with the test data from the TCM pilot plant. The simulation results of CO₂ loading and
254 capture level under two different feed conditions were compared with the data of pilot plants in 2014 and 2015.
255 The CO₂ loading in MEA solvent and the percentage CO₂ capture level is calculated using Eq. (22) and Eq. (23)
256 [33].

257

$$CO_2 \text{ loading (mol } CO_2/\text{mol MEA)} = \frac{[CO_2] + [HCO_3^-] + [CO_3^{2-}] + [MEACOO^-]}{[MEA] + [MEA^+] + [MEACOO^-]} \quad (22)$$

258

$$\text{Capture level} = \left(\frac{y_{CO_2in} - y_{CO_2out}}{y_{CO_2in}} \right) \times 100\% \quad (23)$$

259

Table 7 shows the comparison between the results of experimental measurement and simulation. From the

260

percentage relative error (PRE) of the simulation results and experimental data, it can be obtained that the model

261

can simulate the pilot plant well.

262

Table 6 Baseline process conditions from TCM CO₂ capture plant [48, 49]

Parameter	2014 Baseline data	2015 Baseline data
Flue gas flow rate (Sm ³ /h)	46970	59430
Lean solvent flow (kg/h)	54900	57434
L/G ratio (kg/kg)	1.17	0.97
Flue gas temperature (°C)	25	29.8
Flue gas pressure (bar)	1.063	1.01
CO ₂ (vol%)	3.7	3.7
O ₂ (vol%)	13.6	14.6
N ₂ (vol%)	79.75	78
H ₂ O (vol%)	2.95	3.7
Lean solvent temperature (°C)	36.5	37
Lean solvent pressure (bar)	1.0313	1.0313
Lean MEA concentration (wt%)	30	31
Lean solvent density (kg/m ³)	1067	1073
Lean CO ₂ loading (mol CO ₂ /mol MEA)	0.23	0.2
Rich CO ₂ loading (mol CO ₂ /mol MEA)	0.48	0.48

TCM Reboiler duty (GJ/t CO ₂)	4.14	3.62
TCM plant CO ₂ capture level (%)	93.5	83.4

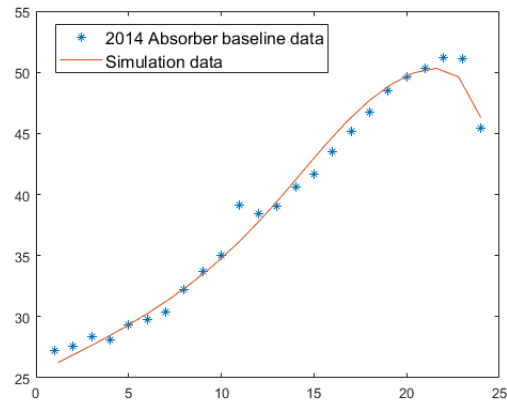
263 Fig.3. and Fig.4. represent the temperature profiles of the liquid phase in the absorber and stripper, respectively.
264 Since there is no temperature profile of the stripper in the 2014 baseline case, only the temperature profile of the
265 absorber is validated[48, 49]. The average deviation of the simulated temperature of the absorber in the 2014
266 baseline case is 0.2°C. The average deviation of the simulated temperature of the absorber and stripper in the 2015
267 baseline case is 4.4°C and 1.8°C, respectively. By comparison, the model prediction deviation of the 2015 baseline
268 case is higher than that of 2014. However, the deviation of the predicted temperature from the data of the TCM
269 pilot plant is still low. The comparison results show that the model can reasonably simulate the operation of
270 absorber and stripper.

271 **Table 7 Results from model validation**

	2014 Baseline	2015 Baseline
Lean loading of the experiment (mol CO ₂ /mol MEA)	0.23	0.20
Lean loading of the model (mol CO ₂ /mol MEA)	0.234	0.21
PRE of lean loading (%)	1.74	5.00
Rich loading of the experiment (mol CO ₂ /mol MEA)	0.48	0.48
Rich loading of the model (mol CO ₂ /mol MEA)	0.489	0.483
PRE of rich loading (%)	1.88	0.63
Reboiler duty of experiment (GJ/t CO ₂)	4.14	3.62
Reboiler duty of the model (GJ/t CO ₂)	4.02	3.57
PRE of reboiler duty (%)	2.9	1.4
CO ₂ capture level of the experiment (%)	93.5	83.4

CO ₂ capture level of the model (%)	90	80.2
PRE of CO ₂ capture level (%)	3.74	3.84

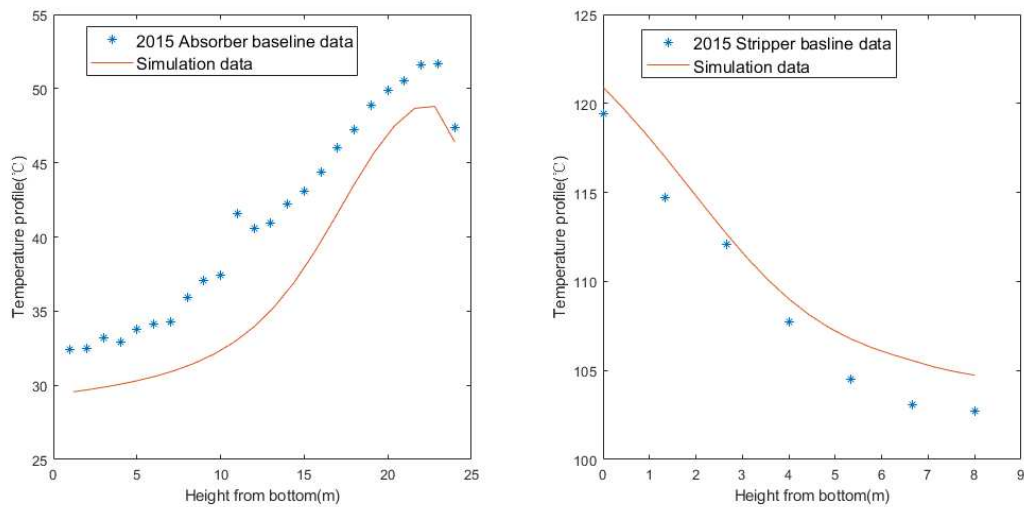
272



273

274

Fig. 3. Simulation results of absorber temperature profile based on baseline data of TCM pilot plant in 2014



275

276

Fig. 4. Simulation results of absorber (left) and stripper (right) temperature profiles based on baseline data of TCM pilot

277

plant in 2015

278

4. Integration of the thermal cracking unit with PCC process

279

4.1. Model scale-up

280

In order to integrate the thermal cracking unit with PCC process, the validated CO₂ capture plant model needs

281 to be scaled up to the size capable of handling the flue gas from the industrial thermal cracking unit. The scale-up
 282 allows the lean solvent flow rate and the dimensions of the absorber and the stripper to be determined.

283 In commercial-scale PCC process research, the generalized Pressure Drop Correlation (GPDC) method is
 284 usually used to scale up the validated pilot-scale model. The pressure drop of the column needs to be assumed
 285 when using the GPDC method, which may result in an inaccurate prediction of the column diameter. Otitoju et
 286 al.[51] proposed a method to predict packed column diameter without assuming pressure drop. This new method
 287 is adopted in this paper to estimate the diameter of the absorber and stripper.

288 Kister et al. [52] correlated the pressure drop when the initial overflow occurs in the packed columns with the
 289 packing factor F_P , as shown in Eq.(24):

$$290 \quad \Delta P_{fl} = 0.115F_P^{0.7} \quad (24)$$

291 This equation is particularly suitable for packing with F_P between 10 and 60 ft⁻¹. When F_P exceeds
 292 60 ft⁻¹, this equation should not be used.

293 The flooding velocity in Eq. (25) is calculated as follows[51]:

$$294 \quad V_{G,fl} = 0.3048 \left[\left(\frac{\rho_G}{\rho_L - \rho_G} \right)^{-0.5} v^{-0.05} F_P^{-0.5} \left\{ A \left(\log \left(\frac{L}{G} \sqrt{\frac{\rho_G}{\rho_L}} \right) \right)^2 \right. \right. \\ \left. \left. + B \left(\log \left(\frac{L}{G} \sqrt{\frac{\rho_G}{\rho_L}} \right) \right) + C \right\} \right] \quad (25)$$

295 Table 8 summarizes the equation that determines the parameters A, B, C in Eq.(25) and their application scope.

296 **Table 8 Expressions for parameters in Eq.(25).**

Parameters	Expression	Range of application
A	$0.07 \ln(\Delta P_{fl}) - 0.11$	$0.5 \leq \Delta P_{fl} \leq 5.0$ inH ₂ O/ft
B	$-0.25 \ln(\Delta P_{fl}) - 0.89$	$0.5 \leq \Delta P_{fl} \leq 1.0$ inH ₂ O/ft
B	-0.89	$1.0 \leq \Delta P_{fl} \leq 5.0$ inH ₂ O/ft
C	$0.12 \ln(\Delta P_{fl}) + 0.71$	$0.5 \leq \Delta P_{fl} \leq 5.0$ inH ₂ O/ft

297 These parameters are determined by the pressure drop of the flooding point, calculated by Eq.(24). Once the

298 physical quantities such as velocity, density, and viscosity of each phase are known, the flooding velocity in the
299 packed column can be calculated. It is generally assumed that the packed column is operated at 60-80% flooding
300 velocity [53]. Taking the intermediate value that the column is operated at 70% flooding velocity. The superficial
301 gas velocity is defined:

$$302 \quad V_G = 0.7V_{G,fl} \quad (26)$$

303 At 70% flooding velocity, the column diameter is defined:

$$304 \quad D = \sqrt{\frac{4G}{\pi V_G \rho_G}} \quad (27)$$

305 The flow rate and compositions of the flue gas are provided in Table 3. Assuming the absorption capacity is 0.2
306 mol CO₂/mol MEA, it can be estimated how much solvent is needed to fulfill 90% capture level in the absorber with
307 30 wt% MEA.

308 The flow rate of lean solvent is calculated using the expression shown in Eq. (28).

$$309 \quad L_{lean} = \frac{Gx_{CO_2}\varphi_{CO_2}}{(\alpha_{rich}-\alpha_{lean})} * \frac{M_{MEA}}{44 * \omega_{MEA}} \quad (28)$$

310 For the stripper, the total solvent flow rate equals the sum of the rich solvent flow rate and the reflux flow rate.

311 The gas flow is equal to the boiling rate to maintain the CO₂ loading in the lean solvent at 0.23 mol CO₂/ mol MEA.

312 Thus, the solvent flow rate of the absorber and stripper are calculated to be 62.58 kg/s and 66.14 kg/s, respectively.

313 The vapour flow rate is 7.6 kg/s.

314 The diameters of the absorber and stripper can be calculated using Eq.(25)-(27). The absorber and stripper are
315 packed with Flexipac 2X with the F_P of 49.8 m⁻¹ (15.179 ft⁻¹) in the TCM pilot plant model. The estimated solvent
316 flow rates and the packing factor in the previous calculation are input to Eq.(25) and Eq.(26). Thus, the superficial
317 gas velocities of the absorber and stripper are calculated to be 1.55 m/s and 1.53 m/s, respectively. Therefore,
318 according to Eq.(27), the diameters of the absorber and stripper are 3.80 m and 2.50 m, respectively. Table 9 shows

319 the calculated data and results of the absorber and the stripper.

320 **Table 9 Capture plant equipment design**

	Absorber	Stripper
Gas flow (kg/s)	24.72	7.60
Liquid flow (kg/s)	62.58	66.14
Packing type	Flexipac 2X	Flexipac 2X
ρ_G (kg/m ³)	1.42	1.02
ρ_L (kg/m ³)	1033.00	1038.00
F_p (ft ⁻¹)	15.18	15.18
v (m ² /s)	0.002	0.0007
A	-0.13	-0.13
B	-0.83	-0.83
C	0.68	0.68
Column diameter (m)	3.80	2.50
Packing height (m)	24.00	10.00

321 4.2. Steady-state integration case studies

322 4.2.1. Case 1: No heat integration of PCC plant into the thermal cracking furnace

323 The temperature of the flue gas at the outlet of the thermal cracking furnace is relatively high, reaching 115.50°C.
324 Before entering the absorber, the flue gas is pretreated to improve the absorption efficiency. The flue gas
325 temperature is cooled to 37°C using cooling water. This is the same as the flue gas temperature in the TCM pilot
326 plant.

327 In the solvent-based carbon capture plant, while CO₂ is absorbed into the MEA solvent, part of the water and
328 MEA will be released from the top of the absorber together with the treated flue gas. After the treated flue gas
329 passes through the wash column, part of the water and MEA are recovered. But the evaporated water and MEA
330 make the PCC process fail to achieve water/MEA balance. To compensate for the material loss, make-up water

331 and make-up MEA are added to the carbon capture plant. The flow rate of make-up water and make-up MEA is
 332 calculated based on the flow rate of those components in the released treated gas. High concentrations of CO₂ can
 333 be obtained from the top of the stripper. The captured CO₂ needs to be compressed and dehydrated to reach the
 334 requirements for storage and transportation. Three-stage compression is used to compress the captured CO₂, and
 335 an intermediate cooler and dehydration module are set. After compression, the pressure of CO₂ is 23 bar and the
 336 temperature is 240.15K (-33 °C). Fig.5 shows a closed-loop model of the carbon capture plant developed using
 337 Aspen Plus®.

338 The components and flow rate of the flue gas shown in Table 3 are used as input into the CO₂ capture model.
 339 The dimensions of absorber and stripper in Table 9 are also input into the model. The lean solvent used for the
 340 absorption contains a CO₂ loading of 0.23 mol CO₂/mol MEA and an MEA concentration of 30 wt%. The
 341 specifications of the large-scale carbon capture plant are listed in Table 10.

342 **Table 10 The specifications of the large-scale capture plant.**

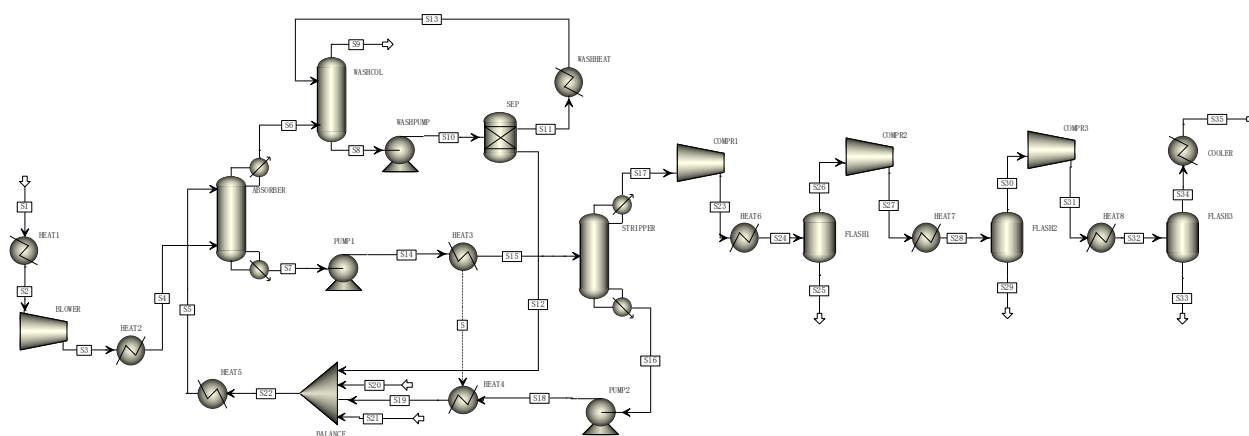
	Case 1
Flue gas flow rate (kg/s)	24.72
CO ₂ content of flue gas(mol%)	7.69
Capture level (%)	90.00
Mass flow rate of CO ₂ captured (kg/s)	2.71
L/G ratio (kg/kg)	2.53
Lean loading (mol CO ₂ /mol MEA)	0.23
Rich loading (mol CO ₂ /mol MEA)	0.53
Reboiler duty (MW)	10.34
Specific reboiler duty (GJ/tonne CO ₂)	3.82

343 From the carbon capture plant result, it can be obtained that the reboiler duty is 10.34 MW when 90% capture
 344 is achieved. The specific reboiler duty of the carbon capture plant is 3.82 GJ/tonne CO₂. Usman et.al[54] studied
 345 the comparative potential of different power generation systems. For the natural gas combined cycle (NGCC)

346 power plant with exhaust gas recirculation, when the molar fraction of CO₂ in flue gas is 6.53%, the specific
 347 reboiler duty is 3.84GJ/tonne CO₂. This result is close to the specific reboiler duty in case 1.

348 The stripper reboiler is the largest energy consumer in the carbon capture plant [55]. Although medium and
 349 high-pressure steam are produced in an ethylene plant. These steam flows are fully allocated therefore leaving no
 350 surplus steam to heat the reboiler. For the no heat integration case study, the heat required by the reboiler of the
 351 PCC process is provided by a low-pressure steam of 130°C, which is purchased at the cost of 0.0019 \$/MJ.

352



353

354

355

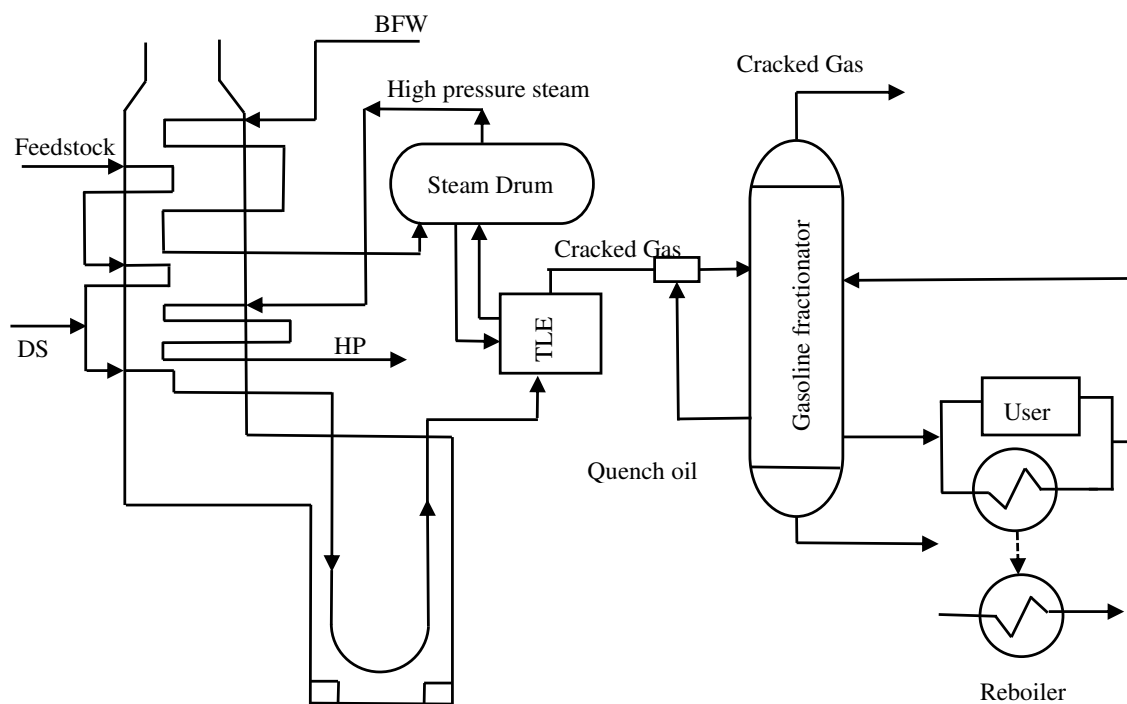
Fig. 5. The closed-loop model of case 1 developed using Aspen Plus®

356 4.2.2. Case 2: Heat integration of gasoline fractionator to the CO₂ capture process

357 In this case study, the excess heat of the gasoline fractionator is supplied to the CO₂ capture process for solvent
 358 regeneration. The primary function of the gasoline fractionator is to cool the cracking gas and initially separate the
 359 gasoline components, diesel components, and fuel oil in the cracking gas. After the cracking gas from TLE is
 360 cooled to about 220-230°C using quench oil in the quencher, it enters the gasoline fractionator. When naphtha is
 361 used for cracking, the temperature at the bottom of the gasoline fractionator is 180-190°C [56]. The quench oil
 362 from the bottom of the gasoline fractionator is sent to the dilution steam system as a heat source to generate dilution
 363 steam. The heat of the cracking gas is recovered. The cracking gas is cooled by quench oil in the gasoline

364 fractionator. When the temperature is reduced to 109°C, the cracking gas leaves from the top of gasoline
365 fractionator and enters the quench water tower for further cooling. As shown in fig.1, (in the pan oil section of the
366 gasoline fractionator), the pan oil is used for heating , including heat exchangers and the materials that need to be
367 heated. The excess heat is recovered with circulating water. This excess heat can be used to heat the reboiler of the
368 stripper.

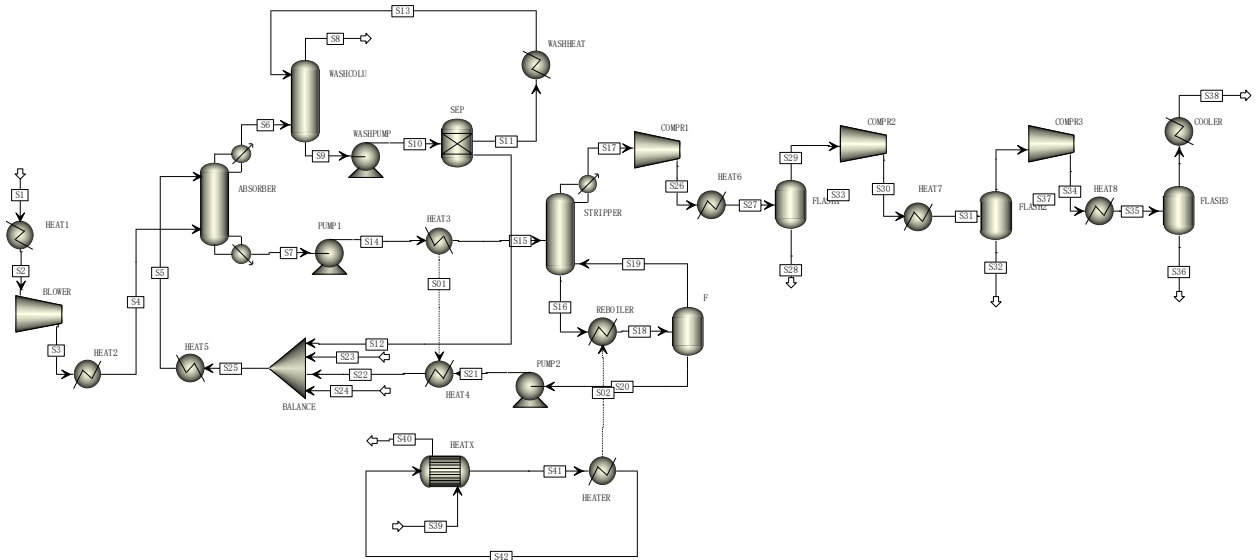
369 To improve the energy recovery of the quench oil system, a stream of hot oil is extracted from the middle of
370 gasoline fractionator to recover heat. A stream of 150°C hot oil is drawn off from the middle of the gasoline
371 fractionator to heat the process water and generate saturated steam with a pressure of 2.7 bar. This saturated steam
372 is used as a heat source for the stripper reboiler in the carbon capture plant. The hot oil is cooled and returned
373 the gasoline fractionator. The schematic diagram of heat integration of the gasoline fractionator in thermal cracking
374 unit with the reboiler of the CO₂ capture process is shown in Fig. 6. The closed-loop model of case 2 developed
375 using Aspen Plus® is shown in Fig. 7.



377 **Fig.6. The heat integration of gasoline fractionator in thermal cracking unit with the reboiler of the**

378 **CO₂ capture process**

379



380

381 **Fig.7. The closed-loop model of case 2 developed using Aspen Plus®**

382 Distillate composition in the cracking gas stream is complex, including heavy cracking gasoline, cracking diesel,
383 and cracking fuel oil. Given this, the method of ordinary paraffin substitution is used to determine the feed
384 components in the simulation. In the gasoline fractionator process, n-decane (NBP=174°C), n-tetradecane
385 (NBP=254°C), and n-docosane (NBP=355°C) are used to describe heavy cracking gasoline, cracking diesel,
386 cracking fuel oil, respectively. The physical property method selected is the Soave Redlich Kwong (SRK) equation
387 of state, which is used to simulate the stream of the gasoline fractionator. The performance of the CO₂ capture
388 process using excess heat of the gasoline fractionator is shown in Table 11. The 150°C hot oil from the gasoline
389 fractionator is used to heat process water and cooled to 139°C before being returned to the gasoline fractionator.

390 In this case, the gasoline fractionator is integrated with the carbon capture process. The hot oil from the gasoline
391 fractionator can directly heat the circulating reboiler condensate into 2.7 bar saturated steam that is then used for

392 solvent regeneration. This approach reduced the energy consumption for solvent regeneration by Case 2 by about
 393 3% compared to Case 1. This shows that by using the excess heat of the gasoline fractionator, the energy
 394 consumption of the PCC process can be reduced. Case 2 also eliminates the cost of purchasing steam and has
 395 potential to reduce the cost of condensate treating equipment.

396 **Table 11 Performance of CO₂ capture process using the excess heat of gasoline fractionator**

	Case 2
Capture level (%)	90.00
CO ₂ captured (kg/s)	2.71
Reboiler duty (MW)	10.04
Specific duty (GJ/tonne CO ₂)	3.70
Saturated steam flow rate (kg/s)	4.58
Temperature of hot oil before heating water (°C)	150
Temperature of hot oil after heating water (°C)	139

397 **5. Economic analysis**

398 The economic analysis of the PCC process was using the Aspen Capital Cost Estimator (ACCE) V11 and the
 399 detailed process flowsheet in Fig.5 and Fig.7. The ACCE V11 is used to calculate the equipment cost, which
 400 included the absorber, the stripper, heat exchangers, and pumps (based on 2018 USD). Li et al.[55] compared the
 401 detailed cost of the MEA-based carbon capture plant with the equipment cost generated by ACCE, and the
 402 difference in the total equipment cost was only 5.2%. Therefore, the ACCE can reasonably estimate the equipment
 403 cost of carbon capture plants.

404 The cost of a CO₂ capture plant includes capital expenditure (CAPEX) and operation expenditure (OPEX). The
 405 CAPEX is calculated from the direct cost of equipment at the PCC plant. The OPEX consists of fixed O&M cost
 406 and variable O&M cost. It is assumed that the fixed O&M cost accounts for 3.5% of the CAPEX of the PCC plant,
 407 which is composed of total maintenance cost and labor cost [55]. The variable O&M cost is caused by energy and

408 chemical consumption during operation, including electricity cost, cooling water cost, steam cost, make-up water
409 cost, and make-up MEA cost.

410 For the two cases, the simulated closed-loop model of the PCC process in Aspen Plus are exported to the ACCE
411 platform. The model blocks are then correctly mapped so that the appropriate costing models are applied to
412 calculate the direct equipment cost of the PCC plant. The calculated results by ACCE for the direct equipment cost
413 of the carbon capture plant based on the two cases considered in this study are listed in Table 12. From the direct
414 equipment cost, it can be found that the stripper cost, cross-heat exchanger cost and heat exchanger cost of case 2
415 are different from case 1. In case 2, the stripper reboiler is heated by saturated steam from the hot oil in the gasoline
416 fractionator. Therefore, case 2 requires a cross-heat exchanger and heat exchanger to heat the reboiler. The resulted
417 in a higher direct equipment cost for case 2 compared to case 1.

418 **Table 12 Direct equipment cost of the large-scale PCC plant of case 1 and case 2**

Equipment	Case 1 (M\$)	Case 2 (M\$)
Absorber	0.42	0.42
Blower	5.74	5.74
Compressors	2.46	2.46
Lean solvent pump	0.01	0.01
Rich solvent pump	0.15	0.15
Wash pump	0.005	0.005
Wash column	0.33	0.33
Wash heat exchanger	0.03	0.03
Separator	0.02	0.02
Stripper	0.86	0.82
HeatX	N/A	0.13
Heaters	0.27	0.29
Flashes	0.05	0.05
Total direct cost (TDC)	10.345	10.455

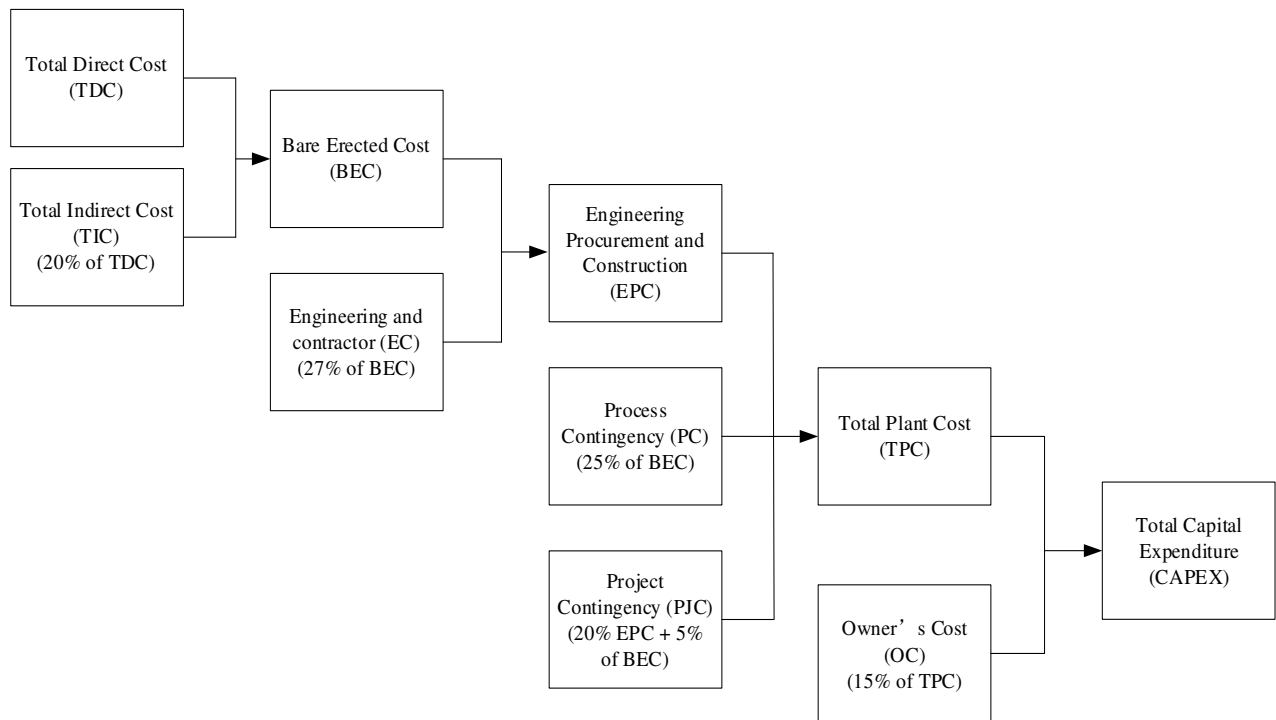
419 It is assumed that the life cycle for the carbon capture plant is 20 years, and the operating time is 8000 hours per
 420 year. The prices of consumables and utility units in the carbon capture process are provided in Table 13. The factory
 421 is set up in East China, and the price is from East China[57].

422 The approach for determining the capital expenditures (CAPEX) is shown in Fig.8. Otitoju et al.[58] has
 423 published the indices used for the CAPEX approach. The CAPEX of the large-scale PCC plant of case 1 and case
 424 2 are provided in Table 14.

425 The total annual cost of a PCC plant is equal to the sum of the annual capital cost (ACC) and the annual operating
 426 costs. The ACC can be obtained by annualizing CAPEX. The formula for calculation is as follows:

$$427 \quad ACC = CAPEX \left(\frac{i(1+i)^n}{(1+i)^n - 1} \right) \quad (29)$$

428 where n is the equipment life, $n=20$; i is the interest rate, $i=10\%$.



429
 430 **Fig.8. The capital expenditures (CAPEX) approach for CO₂ capture plant[58]**

431 **Table 13 The price of consumables and energy**

Description	Value
Electricity (\$/kWh)	0.0762
Low-pressure Steam (\$/MJ)	0.0019
MEA make-up (\$/tonne)	1512.4
Water make-up (\$/tonne)	0.62
Cooling water (\$/tonne)	0.23
Refrigerant - Propane (\$/tonne)	42347.2
Operating time per year (hour)	8000
Exchange rate in 2018 (\$/yuan)	0.15124

432 The CO₂ capture cost is an important economic indicator to evaluate the cost of the PCC process. Without
433 considering the transportation and storage costs of CO₂, the calculation equation is shown in Eq.(30):

$$434 \quad C_c = \frac{E_a + OM_a}{C_{cm}} \quad (30)$$

435 **Table 14 CAPEX of the large-scale PCC plant of case 1 and case 2**

	Case 1 (M\$)	Case 2 (M\$)
Total direct cost (TDC)	10.345	10.455
Total indirect cost (TIC)	2.069	2.091
Bare erected cost (BEC)	12.414	12.546
Engineering and contractor (EC)	3.352	3.387
Engineering procurement and construction (EPC)	15.766	15.933
Process contingency (PC)	3.104	3.137
Project contingency (PJC)	3.774	3.814
Total plant cost (TPC)	22.644	22.884
Owner's cost (OC)	3.397	3.433
Total capital expenditure (CAPEX)	26.041	26.317

436 Carbon credit is a permit that allows a company to emit a certain amount of CO₂ or other greenhouse gases.

437 Industries that cannot reduce CO₂ emissions can purchase credits from other sectors that can reduce more CO₂
 438 emissions than required through carbon credit trading [59]. Recently, the United States and other countries
 439 announced carbon credit for the capture and storage of CO₂. The range of carbon credit obtained from Mokheimer
 440 et al. [60] is from 11.7 to 50 USD/t CO₂. In this paper, 20 USD/t CO₂ is chosen to observe the impact of carbon
 441 credit on the cost of carbon capture. When considering carbon credits, the cost of carbon capture is calculated as
 442 shown in Eq.(31):

$$C_{cc} = \frac{E_a + OM_a}{C_{cm}} - V_{CC} \quad (31)$$

444 A summary of the economic benefits of the carbon capture plant is listed in Table 15. Among the variable O&M
 445 costs, the cost of make-up water is much lower than other consumables. This is because the water and the MEA in
 446 the absorbed flue gas are recovered before the flue gas is discharged, as shown in Fig 2. This operation can reduce
 447 the amount of make-up water and make-up MEA. At the same time, the price of make-up water is much lower
 448 than the price of make-up MEA, thus the cost of make-up water is lower than other consumables. In case 2, the
 449 steam required for reboiler heating is generated from the hot oil of the gasoline fractionator. Therefore, the low
 450 pressure steam cost of case 2 is lower than that of case 1. The CO₂ capture cost is \$80.03/tonne with purchased
 451 steam for heating, while the capture cost is \$70.41/tonne using excess heat of the gasoline fractionator. When
 452 considering carbon credits, the CO₂ capture cost of the two integration schemes is \$60.03/tonne and \$50.41/tonne,
 453 respectively.

454 **Table 15 Summary of the economic performance of the large-scale PCC plant of case 1 and case 2**

Description	Case 1	Case 2
CAPEX (M\$)	26.041	26.317
ACC (M\$/yr)	3.059	3.091
Fixed O&M cost (M\$/yr)	0.911	0.921
Variable O&M cost	Electricity (M\$/yr)	0.643

Cooling water(M\$/yr)	0.464	0.276
Low-pressure steam (M\$/yr)	1.139	0.548
Refrigerant - Propane(M\$/yr)	0.001	0.001
Water make-up (\$/yr)	223.62	93.45
MEA make-up (\$/yr)	62.55	59.21
Total annual cost (M\$/yr)	6.24	5.49
CO ₂ capture cost (\$/tonne CO ₂)	80.03	70.41
CO ₂ capture cost with carbon credit (\$/tonne CO ₂)	60.03	50.41

455 Kangkang Li et al. [55] studied the technical and economic performance of the post-combustion capture process
456 based on MEA and compared the carbon capture cost with other publications. The carbon capture cost of the
457 published study ranges from 62-95.2 \$/tonne CO₂. By comparing the cost of two carbon capture cases, the cost of
458 the basic integration of PCC into the thermal cracking furnace is within a reasonable range. Furthermore, when
459 the excess heat of the gasoline fractionator is used to heat the reboiler, the CO₂ capture cost can be significantly
460 reduced.

461 **6. Conclusions**

462 A detailed technical and economic evaluation of a solvent-based PCC plant for a commercial ethylene plant
463 have been performed in this paper based on two integration strategies-namely no heat integration and heat
464 integration of gasoline fractionator. The composition and flow rate of the flue gas in the thermal cracking furnace
465 are obtained by CFD method. The steady-state model of the PCC plant based on MEA solvent is developed and
466 validated with experimental data collected in 2014 and 2015 at the TCM pilot plant. Furthermore, the PCC plant
467 model is scaled up to treat flue gas from a commercial scale thermal cracking unit.

468 The reboiler of the stripper consumes a significant quantity of energy for solvent regeneration in the carbon
469 capture process. To quantify and reduce this energy consumption, we conduct two integration cases to compare
470 the impact of different heat sources on the energy consumption and cost of CO₂ capture. In the first case, the heat

471 to the reboiler is supplied by steam purchased from a nearby industrial zone. In the second case, the hot oil of the
472 gasoline fractionator is used to heat the circulating condensate into saturated steam. Technical and economic
473 analysis show that heat integration of gasoline fractionators in the thermal cracking unit with the CO₂ capture
474 process could reduce the energy consumption and the capture cost. This study has great potential to inspire
475 researchers worldwide towards research on carbon capture for petrochemical industry.

476

477 **Acknowledgements**

478 This work was supported by the National Natural Science Foundation of China (Basic Science Center Program:
479 61988101), the National Science Fund for Distinguished Young Scholars (61925305), Shanghai Science and
480 Technology Committee (19160712100), the National Natural Science Foundation of China (61973124), and
481 National Key Research & Development Program - Intergovernmental International Science and Technology
482 Innovation Cooperation Project (2021YFE0112800).

OH-	0	0	0	0	0	0	0	0	0	0	0	0	0	0	0	0	0	0	0
HCO3-	0	0	0	0	0.0 17	0	1.5 0	0.0 043	0	0.0 043	0	0.0 022	0	0	0.0 96	0.0 22	0	0	0.0 22
CO3-2	0	0	0	0	0.0 80	0	1.2 3	0	0	0.0 001	0	0	0	0	0.0 04	0.0 54	0	0	0.0 54
MEA +	0	0	0	0	2.9 97	0	7.9 9	0.0 059	0	0.0 06	0	0.0 058	0	0	2.9 1	2.9 7	0	0	2.9 7
MEAC OO-	0	0	0	0	4.7 17	0	6.5 9	0.0 02	0	0.0 02	0	0.0 055	0	0	4.7 0	4.7 5	0	0	4.7 5
N2	18. 12	18. 12	18. 12	18. 12	0	18. 12	0	0	18. 12	0	0	0	0	0	0	0	0	0	0
O2	1.1 0	1.1 0	1.1 0	1.1 0	0	1.1 0	0	0	1.1 0	0	0	0	0	0	0	0	0	0	0

486

487 Table A2

488 Results for mass fraction and mole flowrate of components in each stream of Fig.5.

	S1	S2	S3	S4	S5	S6	S7	S8	S9	S10	S11	S12	S13	S14	S15	S16	S17	S18	S19
Mass Fraction																			
MEA	0	0	0	0	0.162	0.0004	0.016	0.0007	0	0.000 7	0	0.003	0	0	0.16	0.16	1	0	0.16
H2O	0.101	0.101	0.101	0.101	0.649	0.116	0.59	0.995	0.11	0.995	1	0.88	0.01 7	0.01 7	0.65	0.65	0	1	0.65
CO2	0.122	0.122	0.122	0.122	0	0.014	0	0	0.014	0	0	0	0.98 3	0.98 3	0	0	0	0	0
H3O+	0	0	0	0	0	0	0	0	0	0	0	0	0	0	0	0	0	0	0
OH-	0	0	0	0	0	0	0	0	0	0	0	0	0	0	0	0	0	0	0
HCO3-	0	0	0	0	0.0004	0	0.034	0.0014	0	0.001 4	0	0.02	0	0	0.002	0.000 5	0	0	0.000 5
CO3-2	0	0	0	0	0.002	0	0.028	0	0	0	0	0.000 8	0	0	0.000 1	0.001 3	0	0	0.001
MEA H+	0	0	0	0	0.072	0	0.18	0.0019	0	0.002	0	0.05	0	0	0.08	0.072	0	0	0.072

MEACO O-	0	0	0	0	0.114	0	0.15	0.0007	0	0.0007	0	0.05	0	0	0.11	0.12	0	0	0.12
N2	0.733	0.733	0.733	0.733	0	0.820	0	0	0.825	0	0	0	0	0	0	0	0	0	0
O2	0.044	0.044	0.044	0.044	0	0.050	0	0	0.050	0	0	0	0	0	0	0	0	0	0
Mole Flow (kmol/s)																			
MEA	0	0	0	0	0.110	0.00015	0.0066	0.00003	0.	0	0	0	0	0	0.11	0.11	1.1e-5	0	0.11
H2O	0.139	0.139	0.139	0.139	1.488	0.142	0.85	0.006	0.14	0.17	0.17	0.005	0.003	0.003	1.48	1.48	0	0.0004	1.49
CO2	0.0683	0.0683	0.0683	0.0683	0	0.0068	0	0	0.0068	0	0	0	0.062	0.062	0	0	0	0	0
H3O+	0	0	0	0	0	0	0	0	0	0	0	0	0	0	0	0	0	0	0
OH-	0	0	0	0	0	0	0	0	0	0	0	0	0	0	0	0	0	0	0
HCO3-	0	0	0	0	0.00028	0	0.015	0	0	0	0	0	0	0	0.002	0.0004	0	0	0.0004
CO3-2	0	0	0	0	0.0013	0	0.012	0	0	0	0	0	0	0	0	0.0009	0	0	0.0009
MEAH+	0	0	0	0	0.048	0	0.076	0.00006	0	0	0	0	0	0	0.047	0.048	0	0	0.048
MEACO O-	0	0	0	0	0.045	0	0.037	0.00005	0	0	0	0	0	0	0.045	0.046	0	0	0.046
N2	0.647	0.647	0.647	0.647	0	0.647	0	0	0.65	0	0	0	0	0	0	0	0	0	0
O2	0.0344	0.0344	0.0344	0.0344	0	0.0344	0	0	0.034	0	0	0	0	0	0	0	0	0	0

489

490 Table A3

491 Results for material and energy flow flowrates in each stream of Fig. 7.

	S1	S2	S3	S4	S5	S6	S7	S8	S9	S10	S11	S12	S13	S14	S15	S16	S17	S18	S19	S20	S21	S22	S23
T (K)	338.2	348.8	303.2	310.2	331.8	308.4	331.8	331.8	306.4	377.2	392.1	313	299.2	394.3	394.3	394.3	394.3	320.6	310.2	310.2	320.6	403.2	403.2

492
493
494

	2	2	2		2		2																
O2	1.10	1.10	1.10	0	1.10	0	1.10	0	0	0	0	0	0	0	0	0	0	0	0	0	0	0	0

Table A4
Results for mass fraction and mole flowrate of components in each stream of Fig.7.

	S1	S2	S3	S4	S5	S6	S7	S8	S9	S10	S11	S12	S13	S14	S15	S16	S17	S18	S19	S20	S21	S22	S23
Mass Fraction																							
MEA	0	0	0	0.162	0	0.016	0	0.016	0.004	0.023	0.14	0	0	0.15	0.01	0.16	0.16	0.16	1	0	0.16	0	0
H2O	0.101	0.101	0.101	0.649	0.112	0.59	0.11	0.903	0.6	0.6	0.67	0.017	0.017	0.67	0.93	0.65	0.65	0.65	0	1	0.65	1	1
CO2	0.122	0.122	0.122	0	0.014	0	0.014	0	0	0.009	0.0001	0.983	0.983	0.008	0.06	0	0	0	0	0	0	0	0
H3O+	0	0	0	0	0	0	0	0	0	0	0	0	0	0	0	0	0	0	0	0	0	0	0
OH-	0	0	0	0	0	0	0	0	0	0	0	0	0	0	0	0	0	0	0	0	0	0	0
HCO3-	0	0	0	0.0004	0	0.034	0	0	0.022	0.016	0.014	0	0	0.0002	0	0.0002	0.0002	0.0005	0	0	0.0005	0	0
CO3-2	0	0	0	0.002	0	0.028	0	0	0.004	0.002	0.002	0	0	0	0	0.0001	0.0001	0.0014	0	0	0.0001	0	0
MEA H+	0	0	0	0.072	0	0.18	0	0.032	0.16	0.14	0.074	0	0	0.007	0	0.08	0.08	0.07	0	0	0.08	0	0
MEACOO-	0	0	0	0.114	0	0.15	0	0.044	0.21	0.21	0.1	0	0	0.1	0	0.11	0.11	0.11	0	0	0.11	0	0
N2	0.733	0.733	0.733	0	0.825	0	0.825	0	0	0	0	0	0	0	0	0	0	0	0	0	0	0	0
O2	0.044	0.044	0.044	0	0.050	0	0.050	0	0	0	0	0	0	0	0	0	0	0	0	0	0	0	0
Mole Flow (kmol/s)																							
MEA	0	0	0	0.110	0	0.0066	0	0.0003	0.0026	0.016	0.107	0	0	0.11	0.0007	0.11	0.11	0.11	1.1e-05	0	0.11	0	0

H2O	0.13 9	0.13 9	0.13 9	1.488	0.14 2	0.85	0.14	0.006	1.47	1.47	1.7	0.0 03	0.0 03	1.7 1	0.23	1.48	1.48	1.48	0	0.00 04	1.49	0. 25	0. 25
CO2	0.06 83	0.06 83	0.06 83	0	0.00 68	0	0.00 68	0	0	0.00 9	0.00 01	0.0 62	0.0 62	0.0 06	0.00 6	0	0	0	0	0	0	0	0
H3O+	0	0	0	0	0	0	0	0	0	0	0	0	0	0	0	0	0	0	0	0	0	0	0
OH-	0	0	0	0	0	0	0	0	0	0	0	0	0	0	0	0	0	0	0	0	0	0	0
HCO3-	0	0	0	0.000 28	0	0.01 5	0	0	0.01 6	0.01 2	0.00 9	0	0	0.0 02	0	0.00 2	0.00 2	0.00 03	0	0	0.00 03	0	0
CO3-2	0	0	0	0.001 3	0	0.01 2	0	0	0.00 4	0.00 04	0.00 1	0	0	0	0	0	0	0	0	0	0.00 1	0	0
MEAH +	0	0	0	0.048	0	0.07 6	0	0.000 06	0.11	0.1	0.05	0	0	0.0 47	0	0.04 7	0.04 7	0.04 8	0	0	0.04 8	0	0
MEAC OO-	0	0	0	0.045	0	0.03 7	0	0.000 05	0.08 8	0.09	0.04	0	0	0.0 45	0	0.04 5	0.04 5	0.04 6	0	0	0.04 6	0	0
N2	0.64 7	0.64 7	0.64 7	0	0.64 7	0	0.65	0	0	0	0	0	0	0	0	0	0	0	0	0	0	0	0
O2	0.03 44	0.03 44	0.03 44	0	0.34 4	0	0.03 4	0	0	0	0	0	0	0	0	0	0	0	0	0	0	0	0

496 **References**

- 497 [1] Olivier J.G., Peters J. Trends in global CO₂ and total greenhouse gas emissions-2020 report. PBL Netherlands
498 Environmental Assessment Agency 2020:1-85.
- 499 [2] Hu A. China's goal of achieving carbon peak by 2030 and its main approaches. Journal of Beijing University of
500 Technology(Social Sciences Edition) 2021;21:1-15.
- 501 [3] Liu C., Jiang X., Dai J., Wu M., Chen R. Overview of the domestic and foreign oil and gas industry development in
502 2020 and outlook for 2021. International Petroleum Economics 2021;29:28-37.
- 503 [4] Song Q., Mu Y., Hou Y., Wang C., Zheng Y. Comparative analysis of the strength of petrochemical industry between
504 China and USA. Chemical Industry and Engineering Progress 2020;39:1607-1619.
- 505 [5] Ni J. In the context of carbon neutrality, what is the pressure of carbon emissions in the chemical industry? China
506 Petroleum and Chemical Industry 2021:22-27.
- 507 [6] Wang M., Lawal A., Stephenson P., Sidders J., Ramshaw C. Post-combustion CO₂ capture with chemical absorption:
508 A state-of-the-art review. Chemical engineering research and design 2011;89:1609-1624.
- 509 [7] Vega F., Baena-Moreno F.M., Gallego Fernández L.M., Portillo E., Navarrete B., Zhang Z. Current status of CO₂
510 chemical absorption research applied to CCS: Towards full deployment at industrial scale. Applied Energy 2020;260.
- 511 [8] Jiang W., Siyuan R., Yijing S., Qizhen L. Research and application of CCUS technology based on“double
512 carbon”background. Journal of Huazhong University of Science and Technology(Natural Science Edition) 2022:1-12.
- 513 [9] Lawal A., Wang M., Stephenson P., Yeung H. Dynamic modelling of CO₂ absorption for post combustion capture in
514 coal-fired power plants. Fuel 2009;88:2455-2462.
- 515 [10] Zhou Y., Yang D. Simulation and optimum design for convection section of ethylene cracking furnace. Chemical
516 Engineering (China) 2010;38:99-102.
- 517 [11] Hottel H.C., Sarofim A.F., Radiative transfer, McGraw-Hill1967.
- 518 [12] Heynderickx G.J., Oprins A.J., Marin G.B., Dick E. Three - dimensional flow patterns in cracking furnaces with
519 long - flame burners. AIChE journal 2001;47:388-400.

- 520 [13] Oprins A.J., Heynderickx G.J., Marin G.B. Three-dimensional asymmetric flow and temperature fields in cracking
521 furnaces. *Industrial & engineering chemistry research* 2001;40:5087-5094.
- 522 [14] Habibi A., Merci B., Heynderickx G. Multiscale modeling of turbulent combustion and NO_x emission in steam
523 crackers. *AIChE journal* 2007;53:2384-2398.
- 524 [15] Hassan G., Pourkashanian M., Ingham D., Ma L., Newman P., Odedra A. Predictions of CO and NO_x emissions
525 from steam cracking furnaces using GRI2. 11 detailed reaction mechanism—A CFD investigation. *Computers & chemical
526 engineering* 2013;58:68-83.
- 527 [16] Hu G., Wang H., Qian F. Numerical simulation on flow, combustion and heat transfer of ethylene cracking furnaces.
528 *Chemical engineering science* 2011;66:1600-1611.
- 529 [17] Stefanidis G.D., Heynderickx G.J., Marin G.B. Development of reduced combustion mechanisms for premixed
530 flame modeling in steam cracking furnaces with emphasis on NO emission. *Energy & fuels* 2006;20:103-113.
- 531 [18] Zhang Y., Qian F., Zhang Y., Schietekat C.M., Van Geem K.M., Marin G.B. Impact of flue gas radiative properties
532 and burner geometry in furnace simulations. *AIChE journal* 2015;61:936-954.
- 533 [19] Ghassabzadeh H., Darian J.T., Zaheri P. Experimental study and kinetic modeling of kerosene thermal cracking.
534 *Journal of Analytical and Applied Pyrolysis* 2009;86:221-232.
- 535 [20] Kumar P., Kunzru D. Modeling of naphtha pyrolysis. *Industrial & Engineering Chemistry Process Design and
536 Development* 1985;24:774-782.
- 537 [21] Ranzi E., Frassoldati A., Granata S., Faravelli T. Wide-range kinetic modeling study of the pyrolysis, partial
538 oxidation, and combustion of heavy n-alkanes. *Industrial & engineering chemistry research* 2005;44:5170-5183.
- 539 [22] Sabbe M.K., Van Geem K.M., Reyniers M.F., Marin G.B. First principle - based simulation of ethane steam
540 cracking. *AIChE journal* 2011;57:482-496.
- 541 [23] Sun W., Saeys M. Construction of an ab initio kinetic model for industrial ethane pyrolysis. *AIChE journal*
542 2011;57:2458-2471.
- 543 [24] Van Geem K.M., Reyniers M.F., Marin G.B., Song J., Green W.H., Matheu D.M. Automatic reaction network
544 generation using RMG for steam cracking of n - hexane. *AIChE journal* 2006;52:718-730.

- 545 [25] Zhang Y., Chen H., Chen C.C., Plaza J.M., Dugas R., Rochelle G.T. Rate-based process modeling study of CO₂
546 capture with aqueous monoethanolamine solution. *Industrial & engineering chemistry research* 2009;48:9233-9246.
- 547 [26] Freguia S., Rochelle G.T. Modeling of CO₂ capture by aqueous monoethanolamine. *AIChE journal* 2003;49:1676-
548 1686.
- 549 [27] Tatarczuk A., Stec M., Więclaw-Solnya L., Krótkia A., Spietz T., Wilk A., Śpiewaka D., Zdeb J., Janikowski J. Pilot
550 plant results for advanced CO₂ capture process using AMP/PZ solvent at Tauron's coal-fired Power Plant. 3rd Post
551 Combustion Capture Conference 2015:1-3.
- 552 [28] Lawal A., Wang M., Stephenson P., Obi O. Demonstrating full-scale post-combustion CO₂ capture for coal-fired
553 power plants through dynamic modelling and simulation. *Fuel* 2012;101:115-128.
- 554 [29] Luo X., Wang M. Study of solvent-based carbon capture for cargo ships through process modelling and simulation.
555 *Applied Energy* 2017;195:402-413.
- 556 [30] Luo X., Wang M. Improving prediction accuracy of a rate-based model of an MEA-based carbon capture process
557 for large-scale commercial deployment. *Engineering* 2017;3:232-243.
- 558 [31] Wang M., Joel A.S., Ramshaw C., Eimer D., Musa N.M. Process intensification for post-combustion CO₂ capture
559 with chemical absorption: A critical review. *Applied Energy* 2015;158:275-291.
- 560 [32] Liu X., Chen J., Luo X., Wang M., Meng H. Study on heat integration of supercritical coal-fired power plant with
561 post-combustion CO₂ capture process through process simulation. *Fuel* 2015;158:625-633.
- 562 [33] Wei M., Qian F., Du W., Hu J., Wang M., Luo X., Yang M. Study on the integration of fluid catalytic cracking unit
563 in refinery with solvent-based carbon capture through process simulation. *Fuel* 2018;219:364-374.
- 564 [34] Wu X., Xi H., Ren Y., Lee K.Y. Power-carbon coordinated control of BFG-fired CCGT power plant integrated with
565 solvent-based post-combustion CO₂ capture. *Energy* 2021;226:1-16.
- 566 [35] Chen X., Wu X., Lee K.Y. The mutual benefits of renewables and carbon capture: Achieved by an artificial
567 intelligent scheduling strategy. *Energy Conversion and Management* 2021;233:1-15.
- 568 [36] Xi H., Liao P., Wu X. Simultaneous parametric optimization for design and operation of solvent-based post-
569 combustion carbon capture using particle swarm optimization. *Applied Thermal Engineering* 2021;184:116287.

- 570 [37] Weigl M.C., Schmidt G. Carbon capture in cracking furnaces. In: Proceedings of the AIChE 2010 Spring Meeting
571 and the 6th Global Congress on Process Safety 2010, Mar 21-25; San Antonio, USA.
- 572 [38] Zhao Z., Chong K., Jiang J., Wilson K., Zhang X., Wang F. Low-carbon roadmap of chemical production: A case
573 study of ethylene in China. *Renewable and sustainable energy reviews* 2018;97:580-591.
- 574 [39] Hu G., Yuan B., Zhang L., Li J., Du W., Qian F. Coupled simulation of convection section with dual stage steam
575 feed mixing of an industrial ethylene cracking furnace. *Chemical Engineering Journal* 2016;286:436-446.
- 576 [40] Hu G., Wang H., Qian F., Van Geem K.M., Schietekat C.M., Marin G.B. Coupled simulation of an industrial naphtha
577 cracking furnace equipped with long-flame and radiation burners. *Computers & chemical engineering* 2012;38:24-34.
- 578 [41] Canepa R., Wang M., Biliyok C., Satta A. Thermodynamic analysis of combined cycle gas turbine power plant with
579 post-combustion CO₂ capture and exhaust gas recirculation. *Proceedings of the Institution of Mechanical Engineers,*
580 *Part E: Journal of Process Mechanical Engineering* 2013;227:89-105.
- 581 [42] Aboudheir A., Tontiwachwuthikul P., Chakma A., Idem R. Kinetics of the reactive absorption of carbon dioxide in
582 high CO₂-loaded, concentrated aqueous monoethanolamine solutions. *Chemical engineering science* 2003;58:5195-
583 5210.
- 584 [43] Aspen Plus® Rate Based model of the CO₂ capture process by MEA using Aspen Plus®. Aspen Technology Inc,
585 Cambridge, MA, USA 2008.
- 586 [44] Onda K., Takeuchi, H., Okumoto, Y. . Mass transfer coefficients between gas and liquid phases in packed column.
587 *Journal of Chemical Engineering of Japan* 1968;1:56-61.
- 588 [45] Bravo J.L., Rocha, J.A. and Fair, J.R. Mass transfer in gauze packings. *Hydrocarbon processing* 1985;64:91-95.
- 589 [46] Bravo J.L., Rocha, J.A., Fair, J.R. A comprehensive model for the performance of columns containing structured
590 packings. *ChemE. Symp. Ser.* 1992: A439.
- 591 [47] Montañés R.M., Flø N.E., Nord L.O. Dynamic process model validation and control of the amine plant at CO₂
592 Technology Centre Mongstad. *Energies* 2017;10:1-36.
- 593 [48] Faramarzi L., Thimsen D., Hume S., Maxon A., Watson G., Pedersen S., Gjernes E., Fostås B.F., Lombardo G.,
594 Cents T. Results from MEA testing at the CO₂ Technology Centre Mongstad: Verification of baseline results in 2015.
595 *Energy Procedia* 2017;114:1128-1145.

- 596 [49] Hamborg E.S., Smith V., Cents T., Brigman N., Falk-Pedersen O., De Cazenove T., Chhaganlal M., Feste J.K.,
597 Ullestad Ø., Ulvatn H. Results from MEA testing at the CO2 Technology Centre Mongstad. Part II: Verification of
598 baseline results. *Energy Procedia* 2014;63:5994-6011.
- 599 [50] Øi L.E., Fagerheim S., Simulation of CO2 Absorption at TCM Mongstad for Performance Data Fitting and
600 Prediction, SIMS Conference on Simulation and Modelling SIMS 2020, September 22-24, Virtual Conference, Finland,
601 2021, pp. 332-337.
- 602 [51] Otitoju O., Oko E., Wang M. A new method for scale-up of solvent-based post-combustion carbon capture process
603 with packed columns. *International Journal of Greenhouse Gas Control* 2020;93:102900.
- 604 [52] Kister H.Z., Gill D.R. Predict flood point and pressure drop for modern random packings. *Chemical Engineering*
605 *Progress* 1991;87:32-42.
- 606 [53] Marx-Schubach T., Schmitz G. Modeling and simulation of the start-up process of coal fired power plants with
607 post-combustion CO2 capture. *International Journal of Greenhouse Gas Control* 2019;87:44-57.
- 608 [54] Ali U., Font-Palma C., Akram M., Agbonghae E.O., Ingham D.B., Pourkashanian M. Comparative potential of
609 natural gas, coal and biomass fired power plant with post - combustion CO 2 capture and compression. *International*
610 *Journal of Greenhouse Gas Control* 2017;63:184-193.
- 611 [55] Li K., Leigh W., Feron P., Yu H., Tade M. Systematic study of aqueous monoethanolamine (MEA)-based CO2
612 capture process: Techno-economic assessment of the MEA process and its improvements. *Applied Energy*
613 2016;165:648-659.
- 614 [56] Wang S., Ethylene plant technology and operation, China Petrochemical Press, China, 2009.
- 615 [57] Wang L., He Q. Technical economic analysis of carbon capture units after combustion. *Technical economic analysis*
616 *of carbon capture units after combustion* 2018;47:1-7.
- 617 [58] Otitoju O., Oko E., Wang M. Technical and economic performance assessment of post-combustion carbon capture
618 using piperazine for large scale natural gas combined cycle power plants through process simulation. *Applied Energy*
619 2021;292.
- 620 [59] McHale M.R., McPherson E.G., Burke I.C. The potential of urban tree plantings to be cost effective in carbon credit
621 markets. *Urban Forestry & Urban Greening* 2007;6:49-60.

622 [60] Mokheimer E.M., Shakeel M.R., Sanusi Y.S., Mahmoud M. Thermo - economic comparative analysis of solar -
623 assisted and carbon capture integrated conventional cogeneration plant of power and process steam. International Journal
624 of Energy Research 2020;44:8455-8479.

625